JOURNAL OF GEOPHYSICAL RESEARCH, VOL. 93, NO. B4, PAGES 2775-2783, APRIL 10, 1988

Compensation of Swells and Plateaus in the North Pacific: No Direct Evidence for Mantle Convection

DAVID T. SANDWELL AND MIRIAM L. RENKIN

Institute for Geophysics, University of Texas at Austin

At intermediate and long wavelengths the ratio of geoid height to topography is sensitive to the depth and mode of compensation. A low geoid/topography ratio (<2 m/km) signifies shallow Airy compensation. A higher ratio (~6 m/km) signifies thermal isostasy and/or dynamic uplift from a mantle plume. A very high geoid/topography ratio (>8 m/km) in conjunction with a poor correlation between geoid height and topography is evidence of mantle convection. After subtracting a reference geoid from the observed geoid, previous studies have found a regular pattern of geoid highs and lows with a characteristic wavelength of 3000-4000 km. Since these geoid highs and lows were poorly correlated with topography and resulted in very high geoid/topography ratios (10-20 m/km), they were believed to reflect the planform of mantle convection. We show that the regular pattern of geoid highs and lows is an artifact caused by truncating the reference geoid at spherical harmonic degree 10. Since the geoid spectrum is "red," the residual geoid is dominated by degree 11. When the harmonics of the reference geoid are rolled off gradually, the regular pattern of geoid highs and lows disappears. In the Northeast Pacific, the new residual geoid reflects the lithosphere age offsets across the major fracture zones. In the Northwest Pacific, the residual geoid corresponds to isostatically compensated swells and plateaus. We have calculated the geoid/topography ratio for 10 swells and plateaus and have found a range of compensation depths. The highest geoid/topography ratio of 5.5 m/km occurs on the flanks of the Hawaiian Swell. Intermediate ratios occur in four areas, including the Midway Swell. These intermediate ratios reflect a linear combination of the decaying thermal swell and the increasing volume of Airy-compensated seamounts. Low geoid/topography ratios occur over the remaining five areas (e.g., Emperor Seamounts), reflecting the absence of a thermal swell. Our findings do not support the hypothesis that the planform of mantle convection is evident in the geoid. We see only indirect evidence of thermal plumes reheating the lower lithosphere.

INTRODUCTION

Even before the relationship between seafloor depth and age was well established, *Bill Menard* [1973] discovered several broad areas in the Eastern Pacific that were too shallow for their age. Moreover, he noted higher than normal gravity anomalies over these areas. To explain these observations as well as the apparent bobbing motions of islands, he proposed that the swells are due to the Pacific plate riding over a bumpy asthenosphere. He related the bumps to the upwelling limbs of convection cells. More recent observations of hot spot swells tend to confirm Bill's ideas. The only part of the model that is still controversial is the relationship of the topography and gravity anomalies to mantle convection. If the anomalies are directly related to mantle convection, then they would disappear if the convection could be stopped. On the other hand, if they are indirectly related, then they would persist after the convection was stopped. *Detrick and Crough* [1978] have proposed such an indirect relationship where the upwelling limb of the convection cell reheats the lower lithosphere. In their model the topography and gravity anomalies are mainly caused by thermal buoyancy forces in the lower half of the lithosphere. Bill's analysis of the subsidence histories of guyots and atolls favors the indirect relationship between topographic swells and mantle convection [*Menard and McNutt*, 1982]. In this study we show that geoid heights in the Pacific can be explained by density anomalies within the lithosphere. Therefore, geoid heights are not direct evidence for or against dynamic support.

Paper number 6B5980.
0148-0227/88/006B-5980$05.00

The relationship between geoid height and topography is useful for determining the mode of isostatic compensation for a specific plateau or swell [*Haxby and Turcotte*, 1978]. A low ratio of geoid height to topography indicates that the topography is supported by thickened crust. An intermediate geoid/topography ratio signifies deeper compensation that can be attributed to lithospheric thinning [*Crough*, 1978] and/or dynamic uplift from the rising limb of a convention cell [*Parsons and Daly*, 1983]. A very high ratio of geoid height to topography or a geoid signal with no corresponding topography is due to density anomalies beneath the lithosphere that are dynamically maintained by mantle convection [*McKenzie et al.*, 1980].

A number of studies have examined the relationship between residual geoid heights and topography in the North Pacific [*Marsh and Marsh*, 1976; *McKenzie et al.*, 1980; *Watts and Daly*, 1981; *Marsh et al.*, 1984; *Watts and Ribe*, 1984; *Watts et al.*, 1985]. They found a regular pattern of geoid highs and lows with a characteristic wavelength of 3000-4000 km. Similar patterns have also been observed in residual geoid heights over other ocean basins [*Bowin and Thompson*, 1984; *Kogan et al.*, 1985]. Some of the highs and lows were found to correlate with bathymetric features; others did not. The regularity of the pattern, as well as the less than perfect correlation with topography, was taken as evidence for mantle convection beneath the Pacific Ocean [*McKenzie et al.*, 1980].

Here we show that the regularly spaced pattern of geoid highs and lows is an artifact caused by improper removal of a longer wavelength reference geoid. In the above studies, the reference geoid was computed from spherical harmonic coefficients up to degree and order 10 (or 12). This sharp cutoff causes artificial undulations to occur at wavelengths of 4000 km (or 3300 km) (i.e., the wavelength of the convective rolls). When the coefficients of the reference geoid are rolled off smoothly rather than truncated abruptly, the regular pattern of geoid highs and lows

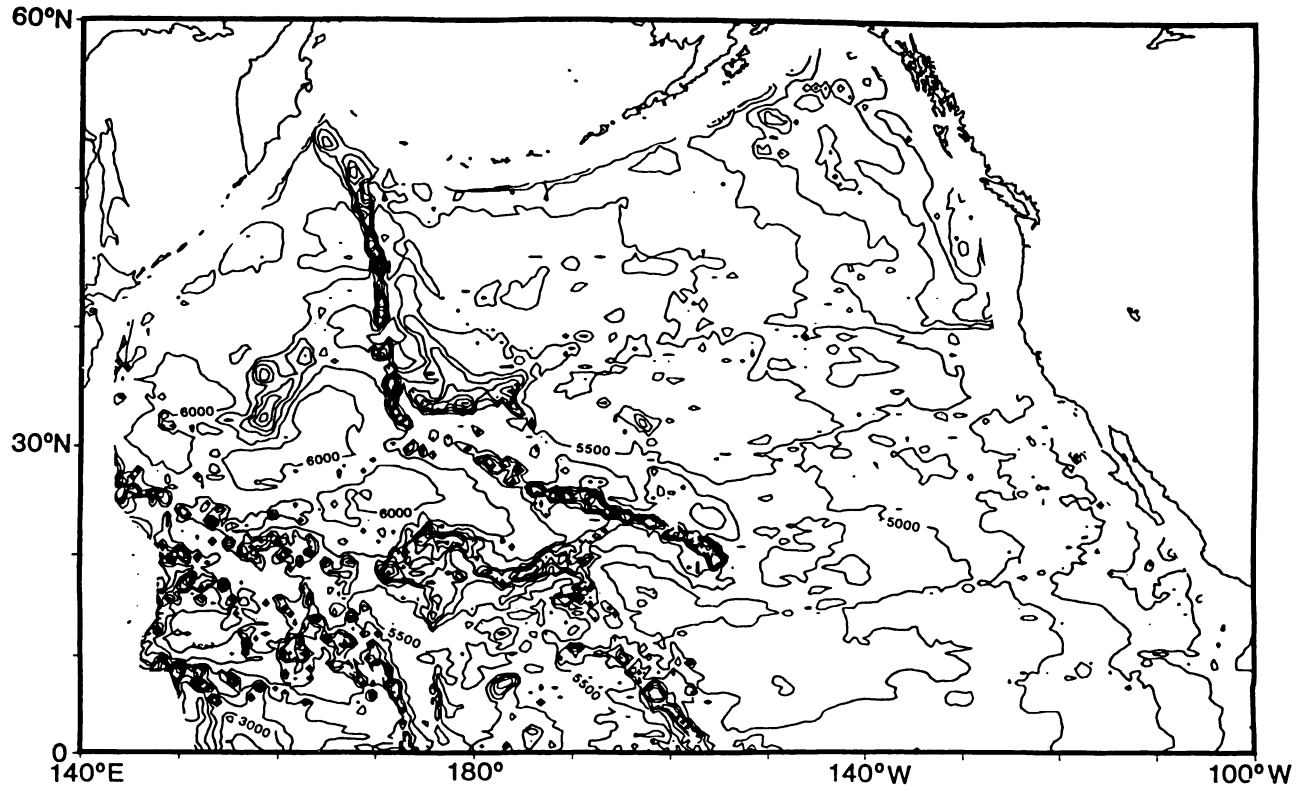

Fig. 1. Sediment-corrected depth of the North Pacific derived from SYNBAPS and seismic reflection data (500-m contour interval). The gradual depth increase toward the west reflects the cooling and contraction of the lithosphere, which is offset by five major fracture zones. Swells and plateaus dominate the topography of the Northwest Pacific.

disappears. The remaining highs and lows correlate well with topographic highs and lows. In the Northeast Pacific there is a high correlation between geoid height and age offsets across fracture zones in agreement with previous studies [*Sandwell and Schubert*, 1980; *Detrick*, 1981]. In the Northwest Pacific, geoid height correlates with swells, plateaus, and basins.

The relationship between geoid height and topography has been investigated for the Hawaiian Swell [*Crough*, 1978; *Sandwell and Poehls*, 1980; *McNutt and Shure*, 1986] and the Line Swell [*Crough and Jarrard*, 1981]. However, there are other features that have not been investigated with this technique because they are more remote and have smaller geoid height and topography signatures. Also, these other areas cannot be analyzed using conventional Fourier transform techniques because they cannot be isolated within a rectangle that is several times wider than a single swell or plateau.

To determine the geoid/topography ratio of small irregularly shaped areas, we band-pass filtered both data sets. We then divided the Northwest Pacific into irregularly shaped areas and plotted geoid height versus topography for each area. The highest ratios occur above the prominent midplate swells such as the Hawaiian Swell and the Line Swell. In these two areas, our results are in agreement with previous studies. A number of features have intermediate geoid/topography ratios reflecting a mixture of a decaying thermal swell signature and the signature of Airy-compensated topography. Finally, we observe a class of swells and plateaus where the geoid/topography ratio is low. These areas (e.g., the Emperor Chain) no longer have a thermal swell signature; they are entirely compensated at shallow depth (~15-20 km). In the North Pacific, geoid/topography ratios do not exceed 6 m/km, suggesting that all topography is compensated within the lithosphere. These findings do not support the hypothesis of *McKenzie et al.* [1980] that the planform of mantle convection is evident in the geoid. We find only indirect evidence that the mantle plumes thin the lithosphere.

SEDIMENT-CORRECTED BATHYMETRY

Uncorrected SYNBAPS bathymetry data [*Van Wykhouse*, 1973] were averaged from 5-min intervals to half degree intervals and corrected for the oceanwide variations in seawater velocity [*Matthews*, 1939]. This interval retains the major bathymetric features. To determine the unloaded basement depth, the data were also corrected for effects of sediment loading.

The sediment thickness chart of *Ludwig and Houtz* [1979] was gridded at half degree intervals and converted to travel time using the velocity/area relations given with the chart. The loading effect of the sediment can be accounted for by a correction that must be added to the bathymetry. It depends not only on the thickness of the sediment column but also on the amount that the sediment load depresses the lithosphere.

Crough [1983] discovered a linear empirical relationship between the sediment correction and the two-way travel time of sound through the sediment column. This empirical relation was determined using six Deep Sea Drilling Project (DSDP) sites and two COST wells in the Atlantic. For the North Pacific, this relationship was checked using density/depth data from DSDP sites 315, 462, and 463. Following *Crough* [1983], the sediment correction was plotted against two-way travel time. The relation is linear and lies within the ±50 m error bar of the relation determined by *Crough* [1983] [*Renkin and Sclater*, this issue]. For the Pacific data the average density and velocity value was used for each layer rather than the velocity measured at the base of the sediment layer as implied by Table 1 of *Crough* [1983].

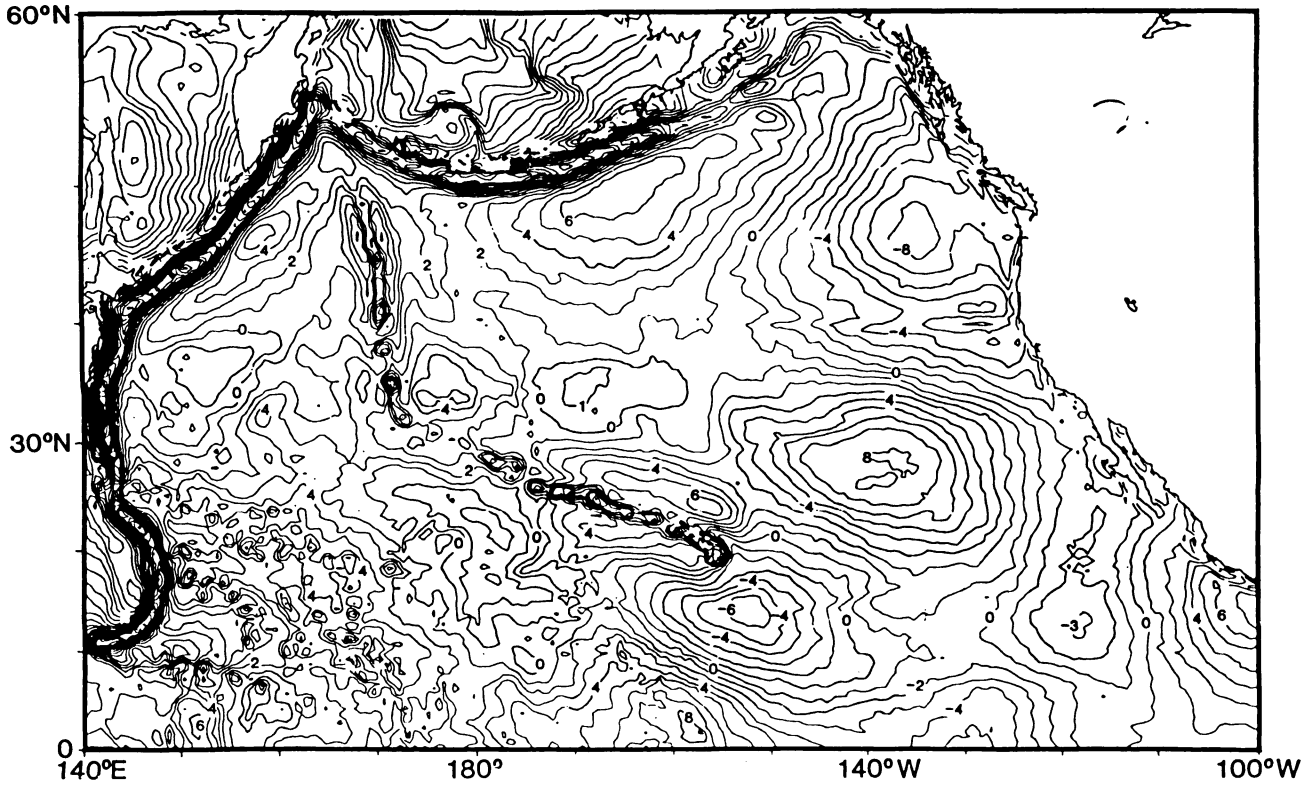

Fig. 2. Residual geoid height (contour interval 2 m) calculated by subtracting spherical harmonic components 2-10 from the observed geoid. The highs and lows, spaced at 1500-2000 km, reflect the sharp cutoff of the reference geoid at degree 10.

Unloaded basement depth, computed by adding the sediment corrections to the bathymetry, was contoured at a 500-m interval (Figure 1). As there are few areas of thick sediments, the sediment-corrected chart shows almost the same features as the uncorrected bathymetry. It is apparent from the corrected bathymetry that the depth increases steadily from the East Pacific Rise until about the longitude of Hawaii at 210°E. Between this longitude and the trenches, the deep basins in the western North Pacific are dominated by a series of large swells, plateaus, and seamount chains.

RESIDUAL GEOID HEIGHT

Gridded geoid heights, derived from Seasat and GEOS 3 satellite altimeter data by *Marsh et al.* [1986], were averaged from quarter degree intervals into half degree intervals. The geoid bears little resemblance to the bathymetry because it is dominated by long-wavelength undulations reflecting deep-seated density anomalies presumably due to mantle convection. The correlation between geoid height and bathymetry can be increased by removing the longest-wavelength geoid undulations. As in previous studies, we are primarily interested in geoid undulations with wavelength shorter than about 4000 km.

The traditional method of removing the long-wavelength components of the geoid is to subtract a low degree and order spherical harmonic representation of the geoid. For example, *McKenzie et al.* [1980] subtracted a reference geoid composed of GEM 7 spherical harmonic coefficients [*Wagner et al.*, 1976] ranging from degree 2 through degree 10. We have approximately reproduced this residual geoid height map by subtracting spherical harmonic coefficients (degrees 2-10) of the model PGS-S4 [*Marsh and Martin*, 1982]. Our residual geoid map is not significantly different from maps presented previously (Figure 2). It shows the regular pattern of geoid highs and lows with a characteristic wavelength of 3600 km. Except for the Hawaiian Swell and Line Islands, there is generally a poor correlation between residual geoid height (Figure 2) and bathymetry (Figure 1). The high (8 m) and low (-6 m) northeast and southeast of Hawaii, respectively, have amplitudes that are much too large to be caused by the subtle variations in seafloor depth. They are artifacts of the method used to remove the long-wavelength geoid.

The artifacts are due to the sharp cutoff of the spherical harmonic coefficients at degree and order 10. This problem is compounded by the fact that the amplitudes in the harmonic coefficients decrease rapidly with increasing spherical harmonic degree [*Kaula*, 1959]. After subtraction, the harmonic coefficients of degree 11 and 12 dominate the residual geoid height map (Figure 2). Sidelobes associated with a sharp cutoff of the coefficients in wave-number space are discussed in text books on Fourier series [e.g., *Bracewell*, 1978].

To minimize the artifacts associated with high-pass filtering the geoid, the coefficients should be rolled off smoothly. We have used a Gaussian function to window the coefficients. Prior to summing the series, coefficients of degree l were multiplied by

$$w_l = exp\left[\frac{-(l-2)^2}{2(\sigma_l - 2)^2}\right] \quad (1)$$

When l reaches σ_l the coefficients are reduced by 0.6. In practice, σ_l was set to 10, and the reference geoid was computed using degrees ranging from 2 to 25. Below, we determine the sensitivity of the results to these parameter values.

The residual geoid computed using this technique (Figure 3) shows that the regular pattern of highs and lows has much lower

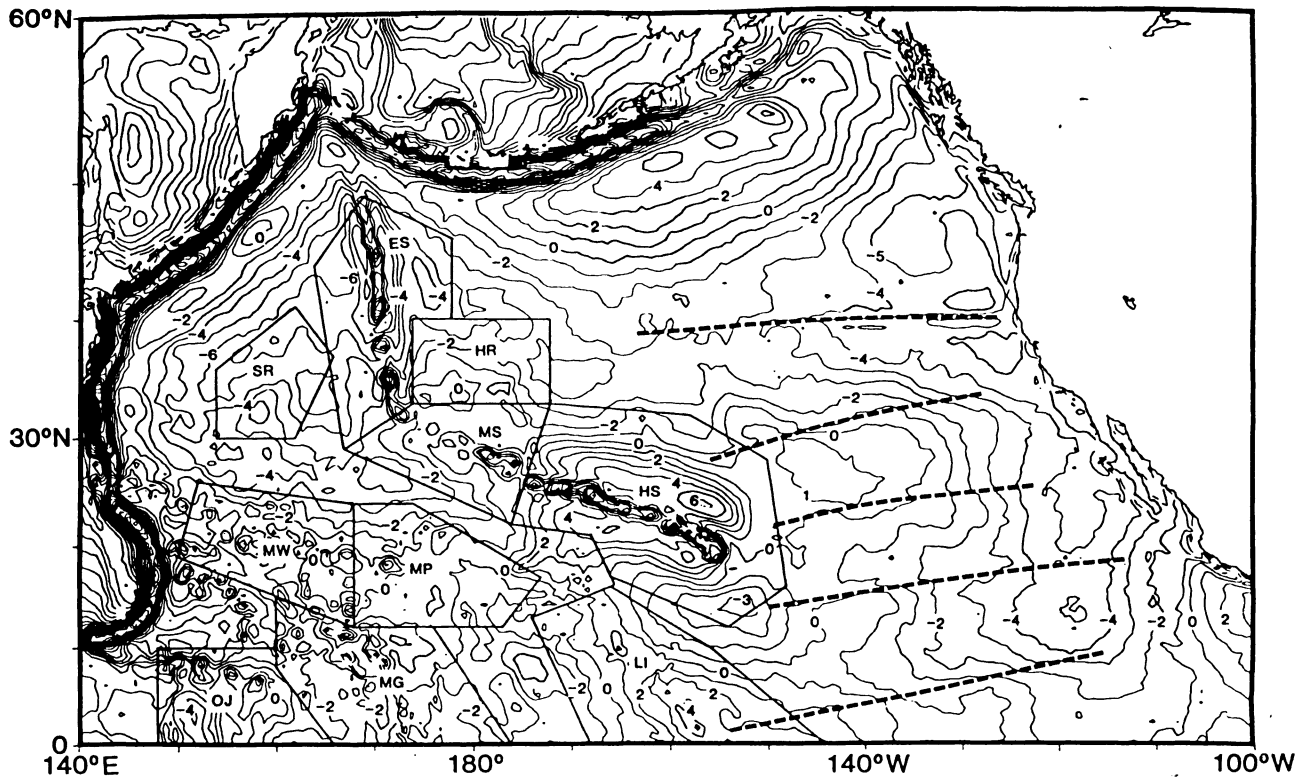

Fig. 3. Residual geoid height (contour interval 2 m) calculated by subtracting spherical harmonic coefficients 2-25 from the observed geoid where the coefficients were rolled off smoothly. The Gaussian window is 1.0 at degree 2 and decreases to 0.6 at degree 10. The highs and lows, spaced at 1500-2000 km no longer dominate the residual geoid. Highs and lows correlate with age offsets of major fracture zones (dashed lines). Outlined areas in the Northwest Pacific contain individual plateaus and swells. HS, Hawaiian Swell; MS, Midway Swell; ES, Emperor Swell; HR, Hess Rise; SR, Shatsky Rise; MW, Marcus-Wake seamounts; MP, Mid-Pacific Mountains; LI, Line Islands; MG, Marshall-Gilbert seamounts; OJ, Ontong-Java Plateau.

amplitude. There is now a generally good correlation between bathymetry (Figure 1) and residual geoid height (Figure 3). The geoid high northeast of Hawaii (1 m) corresponds to the younger section of lithosphere between the Murray and Molokai fracture zones (dashed lines) in accordance with the geoid height versus age relation. The geoid low southeast of Hawaii (-3 m) corresponds to the deep area of seafloor lying between the Hawaiian Swell and the Line Islands. Moreover, this geoid low no longer overprints the southeast end of the Hawaiian Swell.

Even using this new technique, there is still a rather poor correlation between geoid height and topography of the East Pacific Rise and also the outer rise topography of the trenches. Seafloor depths generally increase with age toward the west (Figure 1). The corresponding decrease is not evident in the residual geoid height map because this long-wavelength trend was removed with the reference geoid. This suggests that the long-wavelength components of the geoid should not be removed when geoid height is correlated with age. Also, one should not subtract the geoid-age relationship and the long-wavelength geoid when computing residual geoid heights. There is a continuous band of geoid highs seaward of the trenches that is due to the small uncompensated flexure signal of the outer rise topography [*McAdoo and Martin*, 1984]. A portion of this signature may also be associated with the high-density downgoing slab.

Apart from the trenches and the East Pacific Rise, there is a good visual correlation between broad elevated areas of seafloor and

TABLE 1. Definitions and Values of Parameters

Parameter	Definition	Value
a	mean earth radius	6731.0 km
d	Moho depth (Q_1)	16.0 km
	Moho depth (Q_2)	12.0 km
D	flexural rigidity	4.0×10^{22} N m
g	acceleration of gravity	9.82 m s^{-2}
G	gravitational constant	6.67×10^{-11} m^3 kg^{-1} s^{-2}
L	thermal compensation depth	70.0 km
ρ_c	crustal density	2800 kg m^{-3}
ρ_m	mantle density	3300 kg m^{-3}
ρ_w	water density	1025 kg m^{-3}
s	seafloor depth	5.0 km

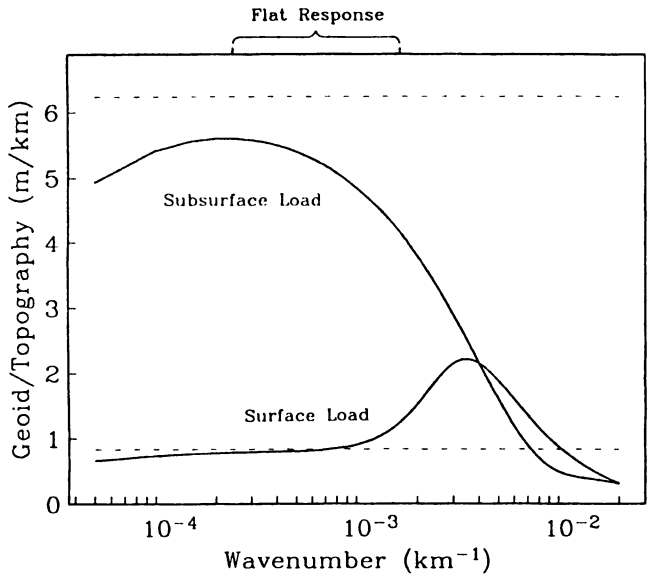

Fig. 4. Geoid/topography transfer functions (solid curves) for surface loading of a thin elastic lithosphere by volcanic rock (16 km compensation depth) and subsurface loading of a thin elastic lithosphere by thermal buoyancy force (70-km compensation depth). Dashed lines are infinite wavelength, flat earth approximations to these transfer functions. Both transfer functions are relatively flat in the wavelength band 600-4000 km (wavelength = 1/wave number).

geoid highs. However, the relationship is not the same for each topographic high. Geoid highs are stronger over the Hawaiian Swell and Line Islands than they are over the Mid-Pacific Mountains and Shatsky Rise. We attribute these differences to two distinct modes of isostatic compensation.

GEOID HEIGHT VERSUS TOPOGRAPHY

The ratio of geoid height to topography depends upon the wavelength of the topography, the mode of isostatic compensation, and the depth of compensation. Following *McNutt and Shure* [1986], we consider only two modes of isostatic compensation, surface loading of an elastic lithosphere by volcanic rock and subsurface loading of an elastic lithosphere by thermal buoyancy forces and/or dynamic support by an upwelling plume.

The ratio of geoid height to topography as a function of wave number, k, for surface loading of an elastic lithosphere is [*McKenzie and Bowin*, 1976; *Banks et al.*, 1977]

$$Q_1(k) = \frac{2ak}{4\pi ak + 1} \frac{2\pi G(\rho_c - \rho_w)}{gk} \left[e^{-2\pi ks} - R(k)\, e^{-2\pi kd} \right] \quad (2)$$

$$R(k) = \left[1 + \frac{D(2\pi k)^4}{g(\rho_m - \rho_w)} \right]^{-1} \quad (3)$$

where definitions and values of parameters are given in Table 1. The first factor in (2) accounts for the sphericity of the earth [*Dorman and Lewis*, 1970].

When the elastic lithosphere is loaded from below by either thermal buoyancy forces or dynamic uplift from a rising plume the ratio of geoid height to topography is [*McNutt and Shure*, 1986]

$$Q_2(k) = \frac{2ak}{4\pi ak + 1} \frac{2\pi G}{gk} \left\{ (\rho_c - \rho_w) \left[e^{-2\pi ks} - e^{-2\pi kL} \right] + (\rho_m - \rho_c) \left[e^{-2\pi kd} - R(k)^{-1} e^{-2\pi kL} \right] \right\} \quad (4)$$

The geoid/topography transfer function for subsurface heating of an elastic lithosphere is similar to this expression [*Sandwell*, 1982].

These two transfer functions are plotted in Figure 4. (Parameter values are given in Table 1.) For surface loading of an elastic lithosphere (Q_1) the ratio of geoid height to topography is relatively constant (1 m/km) at long wavelengths (wavelength = 1/wave number). Near the flexural wavelength the ratio increases to 2 m/km. At much shorter wavelengths the ratio decreases because of upward continuation through the water column.

For an elastic lithosphere loaded from below (Q_2) the ratio of geoid height to topography is relatively high (5.5 m/km) at long wavelengths and then decreases as the wavelength approaches the flexural wavelength [*Sandwell*, 1982]. The effect of the earth's sphericity is to reduce the ratio of geoid height to topography at the longest wavelengths.

The common feature of both transfer functions is that for wavelengths greater than the flexure (~600 km), the ratio of geoid height to topography depends only on compensation depth. The infinite wavelength, flat earth approximations [*Haxby and Turcotte*, 1978] to these two transfer functions are shown as dashed lines on Figure 4. The infinite wavelength approximation agrees well with the surface loading transfer function (Q_1) for wavelength greater than 600 km. It overestimates the subsurface loading transfer (Q_2) function by about 20% at wavelengths greater than 600 km. The important result is that both transfer functions are relatively flat between wavelengths of 600 and 4000 km. Thus, if both the geoid height and topography maps are band-pass filtered to reject components outside this range, then the observed ratio of geoid height to topography can be analyzed in the space domain. The major advantage of space domain analysis is that we can analyze a small, irregularly shaped area enclosing a single swell or plateau.

DATA ANALYSIS

In addition to removing the longest-wavelength components in the geoid, both the geoid and topography were low-pass filtered. Each data set was convolved with a Gaussian-shaped function

$$f(r) = exp\left[\frac{-r^2}{2\sigma^2} \right] \quad (5)$$

where r is distance and σ is the half-width at the filter. A value for σ of 95 km was used to attenuate wavelengths shorter than 600 km. After filtering, only every 36th point was kept. These remaining points, on a 3° grid, are statistically independent. It should be noted that this low-pass filter removes the components of the topography and geoid height that reflect lithospheric flexure. Therefore we were unable to determine the flexural rigidity of the lithosphere for each swell and plateau.

Plots of geoid height versus topography were constructed for selected areas (Figure 3) of the North Pacific seafloor from the smoothed decimated data sets. They are the Hawaiian Swell, the Shatsky Rise, the Mid-Pacific Mountains, the Marshall-Gilbert Islands, the Line Islands, the Marcus-Wake Islands, the Ontong-Java Plateau, the area around Midway Island, and the Emperor Seamounts. The areas were chosen to include parts of the basins

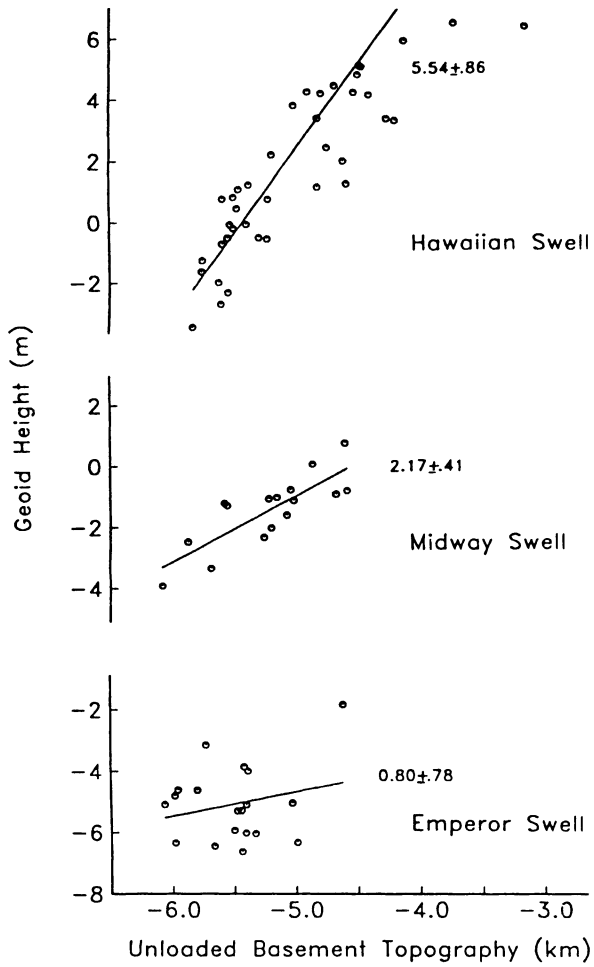

Fig. 5. Geoid height versus basement topography (after low-pass filtering) for the Hawaiian Swell, Midway Swell, and Emperor Swell. Straight lines are least squares fit to the data. The slope and slope uncertainty (in meters per kilometer) appear to the right of each line. The decrease in slope along the Hawaiian-Midway-Emperor Swell reflects the decay of the thermal perturbation of the lower lithosphere resulting in the dominance of the shallow-compensated seamounts.

surrounding a positive feature so that the geoid and topography information on the flanks of the feature would be included. The trench outer rises, which have a high geoid but little topographic signal, have been avoided.

The plots of geoid height versus topography are shown in Figures 5-7. Lines were fit to the data by a least squares method, and slope (i.e., geoid/topography ratio) with error bars was calculated. The Hawaiian Swell and the Line Islands plots show evidence of two distinct geoid/topography ratios, indicating two distinct modes of compensation. The lower geoid/topography ratio corresponds to the shallow compensated seamounts while the higher geoid/topography ratio reflects the deep compensation of the thermal swell. Over the Hawaiian Swell area, two ratios can be distinguished because the seamounts are generally shallower than the swell. To extract the Hawaiian Swell signature, the straight line was fit only to depths greater than 4.8 km. In the other areas, including the Line Islands, the two ratios cannot be completely separated. We interpret the intermediate ratios in these areas as a linear combination of the high ratio due to a thermal swell and the low ratio due to seamounts.

Slopes and slope uncertainties for each area are plotted in Figure 8 along with the geoid/topography transfer functions for Airy and thermal compensation. The characteristic wavelength (1/wave number) for each area was taken as 2 times the half width of the swell or plateau. The geoid/topography ratios fall into three general groups. The Hawaiian area has the highest ratio of 5.54±0.86 m/km. The Line Islands, the Midway region, the Hess Rise and the Marcus-Wake Islands all have similar ratios between 2.06±0.51 m/km and 2.47±0.34 m/km. The lowest ratios correspond to the Ontong-Java Plateau, the Shatsky Rise, the Mid-Pacific Mountains, the Emperor Seamounts, and the Marshall-Gilbert Islands, with values ranging from 1.66±0.44 m/km to 0.50±0.41 m/km.

EFFECTS OF THE BAND-PASS FILTER

To determine the effects of the band-pass filter on the results, we recomputed the geoid/topography slopes and uncertainties for a variety of filters. We have also determined the importance of the sediment unloading correction. The results are given in Table 2. Slopes and uncertainties in column 2 were calculated using the filters and sediment correction described above. The low-pass filter has a cutoff wavelength of 600 km, while the high-pass filter has a smooth cutoff at 4000 km. No sediment correction was used to compute the results in columns 3-6. A comparison of slopes and uncertainties in columns 1 and 2 shows that the *sediment* correction is unimportant.

To determine the effects of the low-pass filter, we varied its cutoff wavelength from 600 km to 400 km to 200 km (not shown). The slopes are unaffected by these filter width changes but the uncertainties decrease as the cutoff wavelength decreases. This is because the narrower filters have more statistically independent points.

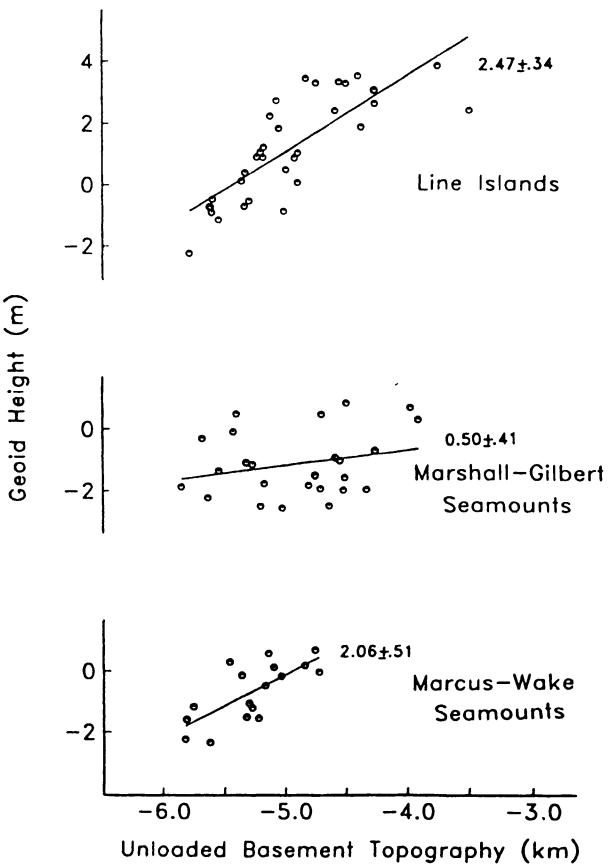

Fig. 6. Geoid height versus topography (low-pass filtered) for the Line Islands, Marshall-Gilbert seamounts, and Marcus-Wake seamounts.

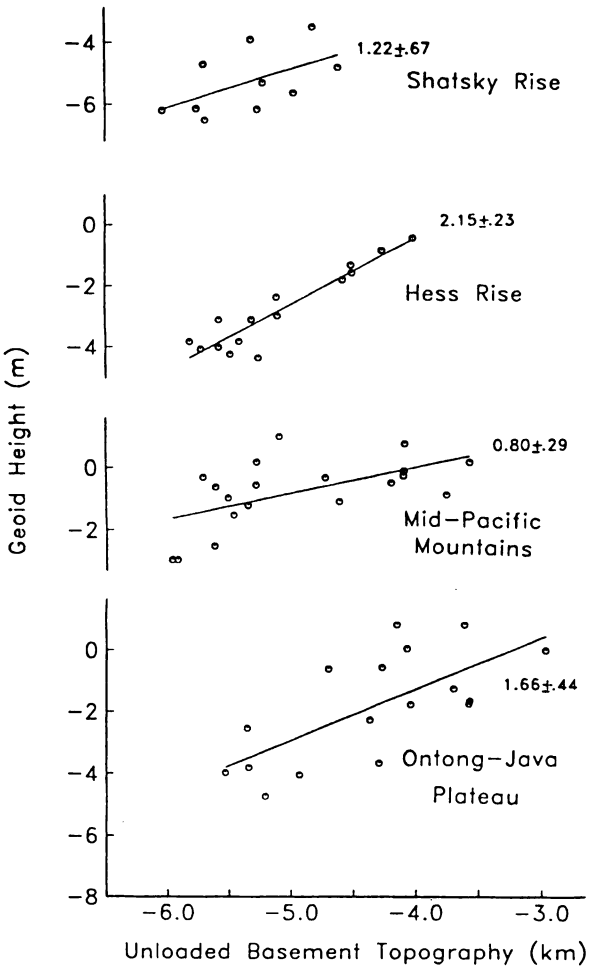

Fig. 7. Geoid height versus topography (low-pass filtered) for the Shatsky Rise, Hess Rise, Mid-Pacific Mountains, and Ontong-Java Plateau.

The high-pass filter has a moderate effect on the results. Except for the Hawaiian Swell, slopes do not change significantly when a sharp high-pass filter (column 5) is used although the uncertainties increase. As described above, the sharp high-pass filter introduces an artificial low at the southeast end of the Hawaiian Chain. This low decreases the geoid/typography correlation as well as the slope. The results are more sensitive to the cutoff wavelength of the high-pass filter. Slopes in column 6 were calculated using a high-pass filter with a smooth cutoff at 6700 km instead of 4000 km. The slopes for the Hawaiian Swell and the Line Swell increase because of this change, although only the Hawaiian slope increase is significant. All of the uncertainties increase from this change, suggesting that the components of the geoid with wavelengths greater than about 4000 km are uncorrelated with the topography of swells and plateaus.

Discussion

In the Hawaiian, Midway, and Emperor areas our results are consistent with the lithospheric reheating model [*Detrick and Crough*, 1978]. A thermal plume is currently thinning the lithosphere under Hawaii, accounting for the large amplitude of the swell. The Midway area which passed over the Hawaiian plume, forming islands between 20 and 40 Ma [*Dalrymple et al.*, 1980], has a decaying swell that is of lower amplitude than the Hawaiian Swell. The swell is absent along the Emperor Chain which passed over the Hawaiian Plume more than 43 m.y. ago. The geoid/topography ratios of these three areas (Figure 5) reflect the decay of the thermal swell. The ratio is highest (5.54±0.86 m/km) over the flanks of the Hawaiian Swell that are uncontaminated by the seamounts. An intermediate ratio (2.17±0.41 m/km) occurs over the Midway Swell, reflecting a mixture of shallow compensated seamounts and the deep compensated thermal swell. The geoid/topography ratio along the Emperor Chain is low, reflecting only the shallow compensation of the seamounts. We will extrapolate our understanding of geoid/topography ratios along the Hawaiian-Midway-Emperor swells to the other swells and plateaus in the Northwest Pacific.

The Line Islands pose an interesting problem. The islands themselves formed in the late Cretaceous (65-80 Ma) and may be synchronous along their length [*Jackson and Schlanger*, 1976]. Rocks dredged from the sides of the islands and guyots show that the volcanoes were reactivated in the middle Eocene (about 42-50 Ma) [*Haggerty et al.*, 1982]. The island chain sits atop a significant swell. The geoid/topography data for the area (Figure 6) suggest the presence of two distinct slopes, though an attempt to remove the shallower slope at 4.8 km ocean depth left too few data to fit a well constrained line. The slope of the entire plot is 2.47±0.34 m/km, intermediate between the two modes of compensation. If interpreted in the same manner as the intermediate Midway Swell, this ratio suggests that the Line Island Swell represents a subsiding thermal plume. Given the middle Eocene age of the last volcanism on the Lines, they should be compared to the southern Emperors, rather than the Midway region. The southern Emperors, however, do not have a visible topographic swell comparable to the Line Swell. The Lines either do not follow the same subsidence/age relation as the Hawaiian-Emperor chain or they have been reheated more recently without volcanic activity.

The Marshall-Gilbert Islands have a similar volcanic history to the Line Islands but are more like the Emperors than the Lines because they do not have a noticeable swell. The area outlined in Figure 3 includes the Marshall Islands, the northern Gilbert Islands, and part of the Nauru Basin. The original volcanism on all of these islands and seamounts is late Cretaceous, evidenced by dredging on the atolls of the Radak chain of the Marshalls

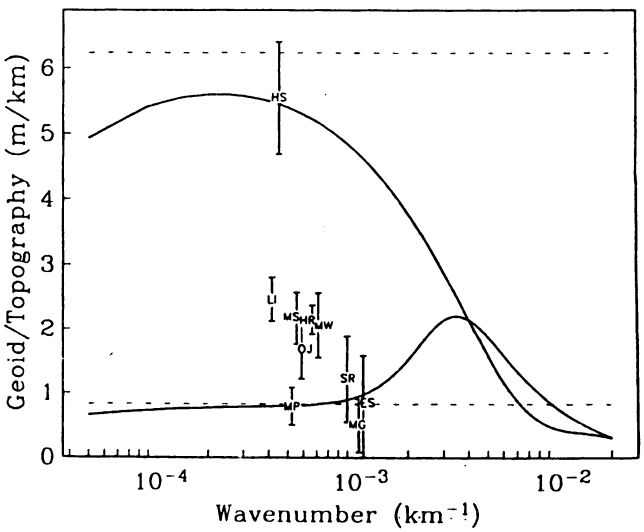

Fig. 8. Geoid/topography ratios and uncertainties for 10 plateaus and swells versus their characteristic wavelength. Transfer functions (solid curves and dashed lines) are the same as Figure 4. All plateaus and swells lie on or between the two transfer functions.

TABLE 2. Dependence of Geoid/Topography Ratio on Band-Pass Filter

	Filter Characteristics				
Sediment Correction	yes	no	no	no	no
Low-Pass	600 km	600 km	400 km	400 km	400 km
High-Pass (σ_l, l_{max})	10, 25	10, 25	10, 25	∞, 10	6, 15
Hawaiian Swell	5.54 ± 0.86	6.18 ± 1.15	4.84 ± 0.57	2.09 ± 1.36	7.38 ± 1.07
Midway Swell	2.17 ± 0.41	2.09 ± 0.35	2.18 ± 0.23	2.24 ± 0.43	2.66 ± 0.90
Emperor Swell	0.80 ± 0.78	0.23 ± 0.65	0.95 ± 0.37	1.33 ± 0.44	0.44 ± 0.60
Line Islands	2.47 ± 0.34	2.62 ± 0.35	2.17 ± 0.24	2.57 ± 0.50	3.12 ± 0.53
Marshall-Gilbert Smts.	0.50 ± 0.41	0.42 ± 0.41	0.53 ± 0.26	0.54 ± 0.26	0.87 ± 0.38
Marcus-Wake Smts.	2.06 ± 0.51	1.95 ± 0.51	1.60 ± 0.36	1.44 ± 0.24	2.30 ± 0.68
Shatsky Rise	1.22 ± 0.67	1.24 ± 0.53	0.82 ± 0.29	0.94 ± 0.40	0.46 ± 0.47
Hess Rise	2.15 ± 0.23	1.78 ± 0.20	1.69 ± 0.13	1.70 ± 0.20	1.10 ± 0.39
Mid-Pacific Mountains	0.80 ± 0.29	0.80 ± 0.30	0.61 ± 0.12	-0.24 ± 0.32	1.14 ± 0.33
Ontong-Java Plateau	1.66 ± 0.44	1.48 ± 0.33	1.57 ± 0.25	1.56 ± 0.34	1.60 ± 0.26

[*Schlanger et al.*, 1981] and by late Cretaceous shallow water debris at DSDP site 462 in the Nauru Basin [*Rea and Theide*, 1981]. Eniwetok atoll has a middle Eocene volcanic edifice [*Ladd et al.*, 1974; *Cole*, 1957; *Kulp*, 1963]. The geoid/topography ratio for the Marshall-Gilbert region is 0.50±0.41 m/km, indicating shallow Airy compensation.

The Marcus-Wake Islands are an elongated cluster of islands and guyots that may be genetically unrelated. Dredge hauls from the Wake Island group found volcanic rocks with lithified Eocene pelagic ooze, suggesting early Tertiary subsidence [*Heezen et al*, 1973]. They have not been drilled, however, and they may have a similar history to the Marshalls and the Lines. There is no clear topographic swell around them, but their geoid/topography ratio is 2.06±0.51 m/km (Figure 6), clearly intermediate. Examination of the geoid map of the area shows that there is a scarp of about 4 m along the north edge of this area. This seems to mark a general transition between higher geoid values (and higher topography) in the southwestern North Pacific to lower geoid values and topography in the northwestern area. The change in the topography is not nearly so sudden as the change in the geoid, however. This rapid change in the geoid accounts for the somewhat steep slope of the geoid/topography plot.

The geoid/topography ratio for the Shatsky Rise (Figure 7) seems to agree with theories based on seismic refraction data that suggest that the oceanic crust is thickened beneath the rise [*Den et al.*, 1969]. The ratio is 1.22±0.67 m/km, indicating simple Airy compensation. *Hilde et al.* [1976] have proposed that it formed by massive basalt outpouring along a leaky fracture zone near a triple junction.

The Hess Rise is a similar broad plateau that is considered to have formed along a spreading ridge by excessive outpourings of basalt. It is middle Cretaceous in age, but underwent an episode of late Cretaceous volcanism [see *Rea and Vallier*, 1983]. There is some evidence for uplift and/or volcanism in the early Tertiary, but this may be related to the formation of the adjacent Emperor Seamounts [*Vallier et al.*, 1983]. The Hess Rise has an intermediate geoid/topography ratio of 2.15±0.23 m/km; similar in value to the Midway Swell (2.17±0.41 m/km). The most likely explanation for this intermediate value is that the Hess Rise may be sitting partly on the Midway Swell.

The Mid-Pacific Mountains are an unusually broad plateau west of the Hawaiian Swell that is topped by at least two chains of seamounts. We have included only the western half of the feature, as the geoid signature of the Hawaiian Swell obscures the eastern half. The Mid-Pacific Mountains show evidence of both Middle and late Cretaceous volcanism at DSDP sites 171, 313, and 463 [*Rea and Vallier*, 1983]. Whatever their origin, spreading center [*Larson*, 1976]; hotspot [*Winterer and Metzler*, 1984], or other, their geoid/topography ratio of 0.80±0.29 m/km (Figure 7) indicates that they are compensated at a shallow depth.

The last feature outlined is the Ontong-Java Plateau. *Carlson et al.* [1980] have suggested that the plateau has both oceanic and continental affinities. Basement is pre-Aptian, and a middle Cretaceous cycle of volcanic sediments was drilled at DSDP sites 288 and 289 [*Shipboard Scientific Party*, leg 30, 1975]. The geoid/topography ratio is 1.66±0.44 m/km. This corresponds to Airy compensation at a depth of 25 km.

SUMMARY

Residual geoid height maps from many previous studies show a regular pattern of highs and lows with a characteristic wavelength of 3000-4000 km. The regularity of the pattern, as well as its less less than perfect correlation with seafloor topography, was taken as evidence for mantle convection beneath the lithosphere. We show that the regular pattern, which mainly consists of spherical harmonic coefficients of degree 11, is an artifact caused by removing spherical harmonic coefficients through degree and order 10. To minimize the sidelobes associated with this sharp high-pass filter, we rolled off the harmonic coefficients using a Gaussian window function. The residual geoid does not have a regular pattern of highs and lows. Instead, we find a high correlation between residual geoid height and seafloor topography.

Using this residual geoid, we calculated the ratio of geoid height to topography for 10 major swells and plateaus in the North Pacific. The highest ratio of 5.5 m/km for the Hawaiian Swell is consistent with an average compensation depth of 70 km. Intermediate ratios, in other areas such as the Midway Swell, are due to a linear combination of the deep compensation of a decaying swell and the shallow compensation of Airy-compensated seamounts. Low geoid/topography ratios (e.g., Emperor Swell) reflect only the shallow compensation of the seamounts. This progression from deep to shallow compensation along the Hawaiian-Midway-Emperor Swell is a consequence of the decay of the thermal swell as excess heat conducts out of the lithosphere.

We expect that a global study of the relationship between geoid height and topography will provide new information concerning the origins of swells and plateaus.

Acknowledgements. We thank John Sclater for encouraging us to do the study. We also thank the reviewers and associate editor for their suggested improvements to the paper. This work was supported by the University of Texas at Austin and the Shell Chair at University of Texas at Austin. UTIG contribution # 681.

REFERENCES

Banks, R. J., R. L. Parker, and J. P. Huestis, Isostatic compensation on a continental scale: Local versus regional mechanisms, *Geophys. J. R. Astron. Soc.*, *51*, 431-452, 1977.

Bowin, C., and G. Thompson, Residual geoid anomalies in the Atlantic Ocean Basin: Relationship to mantle plumes, *J. Geophys. Res.*, *89*, 9905-9918, 1984.

Bracewell, R. N., *The Fourier Transform and Its Applications*, 444 pp., McGraw-Hill, New York, 1978.

Carlson, R. L., N. I. Christensen, and R. P. Moore, Anomalous crustal structures in oceanic basins: Continental fragments and oceanic plateaus, *Earth Planet. Sci. Lett.*, *51*, 171-180, 1980.

Cole, W. S., Larger foraminifera from Eniwetok Atoll drill holes, *U.S. Geol. Surv. Prof. Pap. 260-V*, 1135-1154, 1957.

Crough, S. T., Thermal origin of mid-plate hot-spot swells, *Geophys. J. R. Astron. Soc.*, *55*, 451-469, 1978.

Crough, S. T., The correction for sediment loading on the sea floor, *J. Geophys. Res.*, *88*, 6449-6454, 1983.

Crough, S. T., and R. D. Jarrard, The Marquesas-Line swell, *J. Geophys. Res.*, *86*, 11,763-11,771, 1981.

Dalrymple, G. B., M. A. Lanphere, and D. A. Clague, Conventional and $^{40}Ar/^{39}Ar$ K-Ar ages of volcanic rocks from Ojin (site 430) Nintoku (site 432), and Suiko (site 433) seamounts and the chronology of volcanic propagation along the Hawaiian-Emperor Chain, *Initial Rep. Deep Sea Drill. Proj.*, *55*, 659-676, 1980.

Den, N., W. J. Ludwig, S. Murauchi, J. I. Ewing, H. Hotta, N. T. Edgar, T. Yoshii, T. Asanuma, K. Hagiwara, T. Sato, and S. Ando, Seismic refraction measurements in the northwest Pacific Basin, *J. Geophys. Res.*, *74*, 1421-1434, 1969.

Detrick, R. S., and S. T. Crough, Island subsidence, hot spots, and lithospheric thinning, *J. Geophys. Res.*, *83*, 1236-1244, 1978.

Dorman, L. M., and B. T. R. Lewis, Experimental isostasy, 1, Theory of the determination of the earth's isostatic response to a concentrated load, *J. Geophys. Res.*, *75*, 3357-3365, 1970.

Haggerty, J. A., S. O. Schlanger, and I. Premoli Silva, Late Cretaceous and Eocene volcanism in the Southern Line Islands and implications for hotspot theory, *Geology*, *10*, 433-437, 1982.

Haxby, W. F., and D. L. Turcotte, On isostatic geoid anomalies, *J. Geophys. Res.*, *83*, 5473-5478, 1978.

Heezen, B. C., J. L. Matthews, R. Catalano, J. Natland, A. Coogan, M. Tharp, and M. Rawson, Western Pacific guyots, *Initial Rep. Deep Sea Drill. Proj.*, *20*, 653-724, 1973.

Hilde, T. W. C., N. Isezaki, and J. M. Wageman, Mesozoic sea floor spreading in the North Pacific, in *The Geophysics of the Pacific Ocean Basin and Its Margin*, *Geophys. Monogr. Ser.*, vol. 19, edited by G. H. Sutton, M. H. Manghnani, and R. Moberly, pp. 205-226, AGU, Washington, D.C., 1976.

Jackson, E. D., and S. O. Schlanger, Regional synthesis, Line Islands Chain, Tuamoto Island Chain, and Manihiki Plateau, Central Pacific Ocean, Initial Rep. Deep Sea Drill. Proj., *33*, 915-927, 1976.

Kaula, W. M., Statistical and harmonic analysis of gravity, *J. Geophys. Res.*, *64*, 2401-2422, 1959.

Kogan, M. G., M. Diament, A. Bulot, and G. Balmino, Thermal isostasy in the South Atlantic Ocean from geoid anomalies, *Earth Planet. Sci. Lett.*, *74*, 280-290, 1985.

Kulp, J. L., Potassium-argon dating of volcanic rocks, *Bull. Volcanol.*, *26*, 247-258, 1963.

Ladd, J. S., W. A. Newman, and N. F. Sohl, Darwin guyot, the Pacific's oldest atoll, *Proceedings, International Coral Reef Symposium 2*; pp. 513-535, Great Barrier Reef Committee, Brisbane, Australia, 1974.

Larson, R. L., Late Jurassic and Early Cretaceous evolution of the western central Pacific Ocean, *J. Geomagn. Geoelectr.*, *28*, 219-236, 1976.

Ludwig, W. J., and R. E. Houtz, Isopach map of sediments in the Pacific Ocean basin and marginal sea basins, Am. Assoc. of Pet. Geol., Tulsa, Okla., 1979.

Marsh, B. D., and J. G. Marsh, On global gravity anomalies and two-scale mantle convection, *J. Geophys. Res.*, *81*, 5267-5280, 1976.

Marsh, B. D., J. G. Marsh, and R. G. Williamson, On gravity from SST, geoid from Seasat, and plate age and fracture zones, *J. Geophys. Res.*, *89*, 6070- 6078, 1984.

Marsh, J. G., and T. W. Martin, The Seasat altimeter mean sea surface model, *J. Geophys. Res.*, *87*, 3269-3280, 1982.

Marsh, J. G., A. C. Brenner, B. D. Becklet, and T. V. Martin, Global mean sea surface based on the Seasat altimeter data, *J. Geophys. Res.*, *91*, 3501-3506, 1986.

Matthews, D. J., *Tables of the Velocity of Sound in Pure Water and Sea Water for use in Echo Sounding and Sound Ranging*, Hydrographic Department, The Admiralty, London, 1939.

McAdoo, D. C., and C. F. Martin, Seasat observations of lithospheric flexure seaward of trenches, *J. Geophys. Res.*, *89*, 3201-3210, 1984.

McKenzie, D. P., and C. Bowin, The relationship between bathymetry and gravity in the Atlantic Ocean, *J. Geophys. Res.*, *81*, 1903-1915, 1976.

McKenzie, D. P., A. B. Watts, B. E. Parsons, and M. Roufosse, Planform of mantle convection beneath the Pacific Ocean, *Nature*, *288*, 442-446, 1980.

McNutt, M., and L. Shure, Estimating the compensation depth of the Hawaiian Swell with linear filters, *J. Geophys. Res.*, *91*, 13,915-13,923, 1986.

Menard, H. W., Depth anomalies and the bobbing motion of drifting islands, *J. Geophys. Res.*, *78*, 5128-5137, 1973.

Menard, H. W., and M. K. McNutt, Evidence for and consequences of thermal rejuvenation, *J. Geophys. Res.*, *87*, 8570-8580, 1982.

Parsons, B., and S. Daly, The relationship between surface topography, gravity anomalies, and the temperature structure of convection, *J. Geophys. Res.*, *88*, 1129-1144, 1983.

Rea, D. K., and J. Thiede, Mesozoic and Cenozoic mass accumulation rates of the major sediment components in the Nauru Basin, western equatorial Pacific, *Initial Rep. Deep Sea Drill. Proj.*, *61*, 549-555, 1981.

Rea, D. K., and T. L. Vallier, Two Cretaceous volcanic episodes in the western Pacific Ocean, *Geol. Soc. Am. Bull.*, *94*, 1430-1437, 1983.

Renkin, M. L., and J. G. Sclater, Depth and age in the North Pacific, *J. Geophys. Res.*, this issue.

Sandwell, D. T., Thermal isostasy: Response of a moving lithosphere to a distributed heat source, *J. Geophys. Res.*, *87*, 1001-1014, 1982.

Sandwell, D. T., and K. A. Poehls, A compensation mechanism for the central Pacific, *J. Geophys. Res.*, *85*, 3751-3758, 1980.

Sandwell, D. T., and G. Schubert, Geoid height versus age for symmetric spreading ridges, *J. Geophys. Res.*, *85*, 7235-7241, 1980.

Schlanger, S. O., J. F. Campbell, J. A. Haggerty, and I. Premoli-Silva, Cretaceous volcanism and Eocene failed atolls in the Radak Chain: Implications for the geological history of the Marshall Islands (abstract), *Eos Trans. AGU*, *62*, 1075, 1981.

Shipboard Scientific Party, *Initial Reports of the Deep Sea Drilling Project*, vol. 30, U.S. Government Printing Office, Washington, D.C., 1975.

Vallier, T. L., W. E. Dean, D. K. Rea, and J. Thiede, Geologic evolution of Hess Rise, central North Pacific Ocean, *Geol. Soc. Am. Bull.*, *94*, 1289-1307, 1983.

Van Wykhouse, R., SYNBAPS (Synthetic Bathymetric Profiling Systems), *Tech. Rep. TR-233*, *Nav. Oceanogr. Office*, Washington, D.C., 1973.

Wagner, C. A., F. J. Lerch, J. E. Brownd, and J. A. Richardson, Improvements in the geopotential derived from satellite and surface data (GEM 7 and 8), *Rep. X-921-76-20*, 11 pp., Goddard Space Flight Cent., Greenbelt, Md., 1976.

Watts, A. B., and S. F. Daly, Long wavelength gravity and topography anomalies, *Annu. Rev. Earth Planet. Sci.*, *9*, 415-448, 1981.

Watts, A. B., D. P. McKenzie, B. Parsons, and M. Roufosse, The relationship between gravity and bathymetry in the Pacific Ocean, *Geophys. J. R. Astron. Soc.*, *83*, 263-298, 1985.

Watts, A. B., and N. M. Ribe, On geoid heights and flexure of the lithosphere at seamounts, *J. Geophys. Res.*, *89*, 11,152-11,170, 1984.

Winterer, E. L., and C. V. Metzler, Origin and subsidence of guyots in Mid-Pacific Mountains, *J. Geophys. Res.*, *89*, 9,969-9,979, 1984.

M. L. Renkin and D. T. Sandwell, Institute for Geophysics, University of Texas at Austin, 8701 Mopac Boulevard, Austin, TX 78759.

(Received February 27, 1986;
revised September 17, 1986;
accepted October 6, 1987.)